Hindawi
International Journal of Antennas and Propagation
Volume 2020, Article ID 8205797, 9 pages
https://doi.org/10.1155/2020/8205797

Research Article

Application of Whale Optimization Algorithm to Inverse Scattering of an Imperfect Conductor with Corners

Kun-Chou Lee[1] **and Pai-Ting Lu**[2]

[1]*Department of Systems and Naval Mechatronic Engineering, National Cheng-Kung University, Tainan 701, Taiwan*
[2]*Vanguard International Semiconductor Corporation, Hsinchu, Taiwan*

Correspondence should be addressed to Kun-Chou Lee; kclee@mail.ncku.edu.tw

Received 4 October 2019; Revised 20 January 2020; Accepted 15 February 2020; Published 27 March 2020

Academic Editor: Claudio Curcio

In this paper, the whale optimization algorithm (WOA) is applied to the inverse scattering of an imperfect conductor with corners. The WOA is a new metaheuristic optimization algorithm. It mimics the hunting behavior of humpback whales. The inspiration results from the fact that a whale recognizes the location of a prey (i.e., optimal solution) by swimming around the prey within a shrinking circle and along a spiral-shaped path simultaneously. Initially, the inverse scattering is first transformed into a nonlinear optimization problem. The transformation is based on the moment method solution for scattering integral equations. To treat a target with corners and implement the WOA inverse scattering, the cubic spline interpolation is utilized for modelling the target shape function. Numerical simulation shows that the inverse scattering by WOA not only is accurate but also converges fast.

1. Introduction

Inverse scattering means to reconstruct the shape or the electrical parameter distribution of an unknown scatterer by using the scattering data or the wave propagation model [1]. Basically, the reconstruction of a target's information is associated with the solution of an inverse problem, which is nonlinear and typically ill-posed [2]. The inverse scattering plays a very important role in different branches of science such as medical tomography, nondestructive testing, object detection, geophysics, ground penetrating radars, remote sensing, atmospheric science, and optics. According to electromagnetic theories [3], the relation between a target and its scattered electromagnetic fields involves complicated integral equations together with Green's functions. Therefore, the solution of an inverse scattering problem is very difficult and time-consuming. Conventionally, the inverse scattering techniques are basically divided into two categories. The first category is based on the physical approximation for reducing the mathematical complexity, such as [4–8]. Although the computation of this category is efficient, it has some restrictions (e.g., convex and smoothness) on the target. A target's information may be lost by using techniques of this category. The second category is based on direct numerical solutions of scattering integral equations, such as [9–13]. Although the target's information is completely retained, the computation of this category is time-consuming and even difficult due to the complicated mathematics and ill-posed problems. As a whole, to improve the numerical computation and to retain the target information are the important considerations of inverse scattering, e.g., [14].

Recently, the metaheuristic optimization algorithms are becoming more and more important in many research fields. A metaheuristic algorithm is inherently a stochastic optimization so that the solution is dependent on the set of random variables generated. There are at least three advantages of applying metaheuristic optimization algorithms to engineering problems. First, it relies on rather simple concepts and is easy to implement. Second, it does not require gradient information. Third, it can bypass local optima. The above advantages make metaheuristic optimization algorithms suitable for a wide range of problems covering different disciplines. Since the solution of an integral equation can be transformed into an optimization

problem, it is a reasonable thinking direction to apply metaheuristic optimization algorithms to inverse scattering [15–18].

This study introduces a new metaheuristic optimization algorithm, which is the whale optimization algorithm (WOA) [19], to solve the inverse scattering problem. The WOA mimics the hunting behavior of humpback whales. The inspiration results from the fact that a whale recognizes the location of a prey (i.e., optimal solution) by swimming around the prey within a shrinking circle and along a spiral-shaped path simultaneously, as shown in Figure 1. The most interesting thing about the whale is its special hunting method, which is the bubble-net feeding. A whale prefers to hunt krill and small fishes close to the surface. It has been observed that this foraging is done by creating distinctive bubbles along a circle as shown in Figure 1. To perform optimization, the spiral bubble-net feeding maneuver is mathematically modeled and transformed into formulas. The details are given in Section 2. To our knowledge, so far, there is still no study of applying the WOA to electromagnetic problems.

In this paper, the WOA is applied to the inverse scattering of an imperfect conductor with corners. Similar to [15–18], the inverse scattering is first transformed into a nonlinear optimization problem. The transformation is based on the scattering integral equation [3] and moment methods [20]. To treat a target with corners, the target shape function is characterized by the cubic spline interpolation [21, 22], but not the Fourier series [15, 16, 18]. The fitness (i.e., objective) function is defined by comparing the scattered electric fields from the guessed and true targets, respectively. Numerical results show that the target's information reconstructed by the WOA is very accurate and the convergence is fast.

In the following, Section 2 introduces the whale optimization algorithm. Section 3 describes its application to inverse scattering. Numerical results are given in Section 4. Finally, the conclusion is given in Section 5. The meanings of notations are summarized as Table 1.

2. Whale Optimization Algorithm

In this section, the WOA [19] is briefly introduced. The WOA is basically an iterative method and will be applied to the inverse scattering in the next section.

The original goal of the WOA is to find an optimal solution that maximizes or minimizes a fitness function. Assume $\vec{\mathbf{X}}$ denotes the location vector (i.e., controlled variables) of a whale (i.e., the fitness function) and $\vec{\mathbf{X}}^*$ is the best location (i.e., optimal solution) obtained so far. By using the WOA, $\vec{\mathbf{X}}$ is efficiently updated so that $\vec{\mathbf{X}}^*$ becomes finally optimal. The WOA contains three main mechanisms, which are shrinking and encircling (exploitation phase), spiral updating (exploitation phase), and searching for prey (exploration phase). They are introduced in the following.

2.1. Shrinking and Encircling. This step belongs to the exploitation phase. The mathematical formulas are

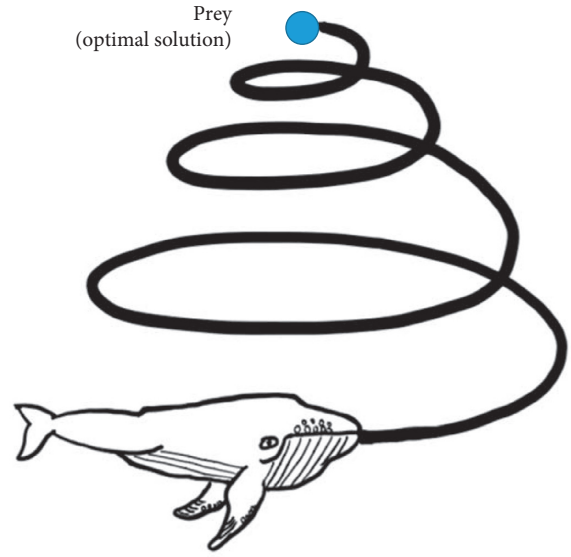

Figure 1: Illustration of a whale swimming around the prey within a shrinking circle and along a spiral-shaped path simultaneously.

$$\vec{\mathbf{D}} = \left|\vec{\mathbf{C}} \circ \vec{\mathbf{X}}^* - \vec{\mathbf{X}}\right|, \tag{1}$$

and

$$\vec{\mathbf{X}}_{\text{new}} = \vec{\mathbf{X}}^* - \vec{\mathbf{A}} \circ \vec{\mathbf{D}}, \tag{2}$$

where $\vec{\mathbf{X}}_{\text{new}}$ is the updated location vector of a whale in the next step. In equations (1)–(2), $\vec{\mathbf{A}}$ and $\vec{\mathbf{C}}$ are randomness coefficient vectors, as now briefly explained. We define

$$\vec{\mathbf{A}} = 2\vec{\mathbf{a}} \circ \vec{\mathbf{r}} - \vec{\mathbf{a}}, \tag{3}$$

and

$$\vec{\mathbf{C}} = 2\vec{\mathbf{r}}, \tag{4}$$

where $\vec{\mathbf{a}}$ is a vector with each component (denoted as a) linearly decreased from 2 to 0 over the whole iterations and $\vec{\mathbf{r}}$ is a vector with random components in the range [0, 1]. From equation (3), it is shown that $\vec{\mathbf{A}}$ is actually composed of random values in the interval $[-a, a]$ where a is decreased from 2 to 0 over the whole iterations. As a result, the fluctuation range of $\vec{\mathbf{A}}$ is affected by $\vec{\mathbf{a}}$ and is then decreased gradually.

2.2. Spiral Updating. This step belongs to the exploitation phase. A spiral equation,

$$\vec{X}_{\text{new}} = \left|\vec{\mathbf{X}}^* - \vec{\mathbf{X}}\right| \cdot e^{bl} \cdot \cos(2\pi l) + \vec{\mathbf{X}}^*, \tag{5}$$

is created for updating the location of a whale. The inspiration is to mimic the helix-shaped movement of a whale. In equation (5), b is a constant for defining the shape of the logarithmic spiral and l is a random number within the range $[-1, 1]$.

2.3. Search for Prey. This step belongs to the exploration phase. We utilize the variation of a vector $\vec{\mathbf{A}}$, which is

Table 1: Meanings of notations.

Notations	Meanings
a	Scalar
$\lvert a\rvert$	Absolute value of scalar a
$\mathbf{A}$	Vector (bold)
$\lvert\vec{\mathbf{A}}\rvert$	Taking absolute value for each element of vector $\vec{\mathbf{A}}$, the result is still a vector
$\vec{\mathbf{A}}\circ\vec{\mathbf{B}}$	Element-by-element multiplication of vectors $\vec{\mathbf{A}}$ and $\vec{\mathbf{B}}$
$\hat{\mathbf{z}}$	Unit vector (bold)

composed of random values, to search for the prey (i.e., optimal location). As $\vec{\mathbf{A}}$ satisfies $|\vec{\mathbf{A}}| \geq 1$, the search agent will move far away from a reference whale. Note that $|\vec{\mathbf{A}}| \geq 1$ means all elements of $\vec{\mathbf{A}}$ (having the same value) are greater than or equal to 1. In such a situation, we update the location of a search agent in the exploration phase according to a randomly chosen search agent, but not toward the currently best location. This mechanism emphasizes exploration and allows the WOA to perform a global search. The mathematical formulas are

$$\vec{\mathbf{D}} = \left|\vec{\mathbf{C}}\circ\vec{\mathbf{X}}_{\text{rand}} - \vec{\mathbf{X}}\right|, \tag{6}$$

and

$$\vec{\mathbf{X}}_{\text{new}} = \vec{\mathbf{X}}_{\text{rand}} - \vec{\mathbf{A}}\circ\vec{\mathbf{D}}, \tag{7}$$

where $\vec{\mathbf{X}}_{\text{rand}}$ is a random location vector chosen from the current population.

Assume the problem is to search for a set of optimal variables $\vec{\mathbf{X}}$ that minimizes a fitness function $g(\vec{\mathbf{X}})$ by using the WOA. As shown in Figure 1, a whale swims around the prey (i.e., optimal location and solution) within a shrinking circle and along a spiral-shaped path simultaneously. The flowchart of the WOA is given in Figure 2. Its iteration procedures are explained in the following.

Step 1: initialize the whale population.

To start the WOA, we first initialize the whale population. Assume there are N_W whales with location vectors denoted as $\vec{\mathbf{X}}_i$, $i = 1, 2, \ldots, N_W$. Components of a location vector represent the controlled variables of the fitness function.

Step 2: generate p and $\vec{\mathbf{A}}$.

For each whale, we generate a random number p within the range $0 \leq p \leq 1$ for deciding the next step. We also generate a random $\vec{\mathbf{A}}$ based on equation (3).

Step 3: check p and $|\vec{\mathbf{A}}|$.

For each whale, we check p and $|\vec{\mathbf{A}}|$, and then update the location vector according to the following rules:

$$\begin{cases} p \geq 0.5, \text{ update by equation (5)}, \\ p < 0.5, \begin{cases} |\vec{\mathbf{A}}| \geq 1, \text{ update by equation (7)}, \\ |\vec{\mathbf{A}}| < 1, \text{ update by equation (2)}. \end{cases} \end{cases} \tag{8}$$

Step 4: calculate the fitness of each whale.

In this step, we calculate the fitness of each whale, i.e., $g(\vec{\mathbf{X}}_i)$, $i = 1, 2, \ldots, N_W$.

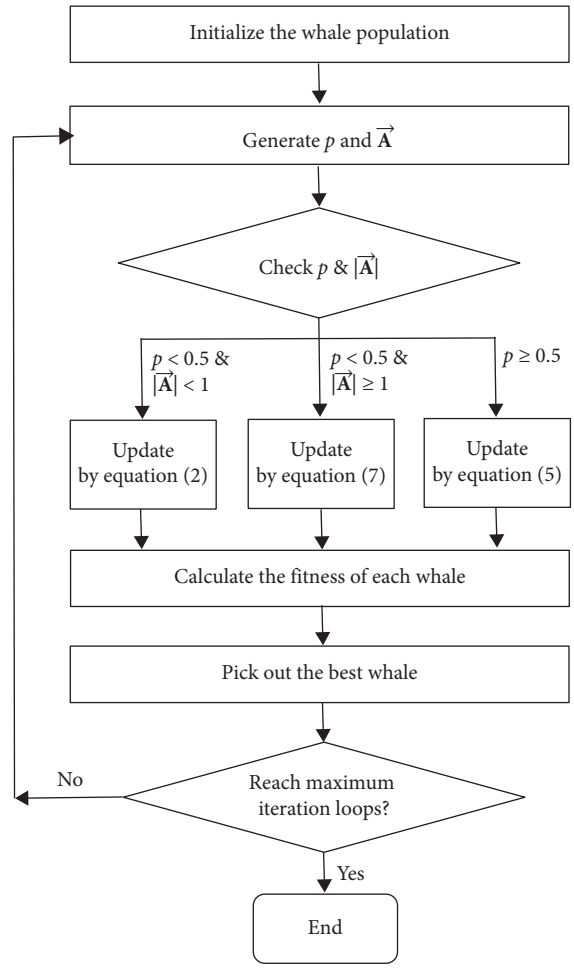

Figure 2: The flowchart of the whale optimization algorithm.

Step 5: pick out the best whale.

Since the problem is to minimize the fitness function, this step becomes to pick out the minimum among $g(\vec{\mathbf{X}}_i)$, $i = 1, 2, \ldots, N_W$. Record the corresponding location vector as $\vec{\mathbf{X}}^*$. Note that the current $\vec{\mathbf{X}}^*$ is the best solution so far.

Step 6: reach maximum iteration loops?

As the iteration has reached the specified maximum number of loops, the WOA stops and $\vec{\mathbf{X}}^*$ is regarded as the final optimal location (i.e., final solution). Otherwise the WOA iteration will continue and go to Step 2.

After the above six steps of WOA iteration procedures, one can obtain the optimal solution (i.e., $\vec{\mathbf{X}}^*$) that minimizes the fitness function $g(\cdot)$.

3. Application to Inverse Scattering

In this study, the above WOA will be applied to inverse scattering. To utilize the WOA, the inverse scattering problem should be first transformed into a minimization problem. Prior to inverse scattering, one should derive the direct scattering formulas. For simplicity without loss of generality, this study considers only the two-dimensional inverse scattering. The target is an imperfectly conducting cylinder with corners. Consider a time-harmonic plane wave with electric field

$$\vec{\mathbf{E}}_i(x,y) = E_i(x,y)\hat{z} = \exp\{-jk_0(x\cdot\cos\alpha + y\cdot\sin\alpha)\}\hat{z}, \tag{9}$$

in free space (permittivity ε_0 and permeability μ_0) incident on a homogeneous cylinder, as shown in Figure 3. In equation (9), (x, y) represents the Cartesian coordinates, k_0 is the wavenumber and α is the incident angle with respect to X-axis. The polar coordinates are denoted as (ρ, ϕ), as illustrated in Figure 3.

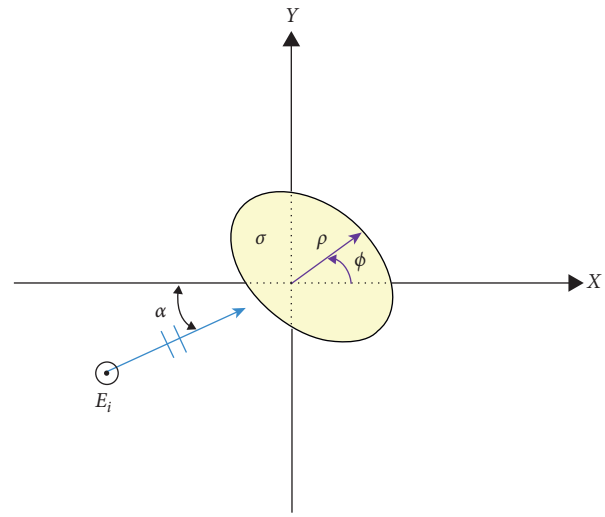

Figure 3: Geometry of a cylinder in free space illuminated by an incident plane wave $\vec{E}_i(x,y) = E_i(x,y)\hat{z}$.

Assume the polar coordinates of the target shape boundary satisfy $\rho = f(\phi)$ where $f(\cdot)$ represents the target shape function. The scattered electric field outside the cylinder is $\hat{z}$-polarized as [3, 15, 17]

$$E_S(x,y) = -\frac{k_0\eta_0}{4}\int_0^{2\pi} H_0^{(2)}\left(k_0\sqrt{[x-f(\phi')\cos\phi']^2+[y-f(\phi')\sin\phi']^2}\right)\cdot\sqrt{[f(\phi')]^2+[f'(\phi')]^2}\cdot J_S(\phi')\mathrm{d}\phi'. \tag{10}$$

In equation (10), η_0 is the intrinsic impedance, $H_0^{(2)}(\cdot)$ is the zero-order Hankel function of the second kind and $J_S(\cdot)$ is the $\hat{z}$-directed surface current density. Note that the notation "prime" indicates the source. Let $\vec{\mathbf{E}}_t(f(\phi),\phi)$ denote the total electrical field. As the target is perfectly conducting, the boundary should obey the condition $\vec{\mathbf{E}}_t(f(\phi),\phi) = 0$. This study considers the imperfectly conducting target. Assume the target conductivity is σ. The boundary should obey the equivalent condition as [23, 24]

$$\hat{\mathbf{n}}\times\vec{\mathbf{E}}_t(f(\phi),\phi) = \hat{\mathbf{n}}\times\left[Z_S\vec{\mathbf{J}}_S(f(\phi),\phi)\right], \tag{11}$$

and

$$Z_S = \sqrt{\frac{j\omega\mu_0}{\sigma}}, \tag{12}$$

where $\hat{n}$ is the outward unit normal vector and Z_S represents the surface impedance. From equations (10)–(12), we have

$$E_i(f(\phi),\phi) = \frac{k_0\eta_0}{4}\int_0^{2\pi} H_0^{(2)}\left(k_0\sqrt{[f(\phi)]^2+[f(\phi')]^2-2f(\phi)f(\phi')\cos(\phi-\phi')}\right)\cdot\sqrt{[f(\phi')]^2+[f'(\phi')]^2} \cdot J_S(f(\phi'),\phi')\mathrm{d}\phi' + J_S(f(\phi),\phi)\sqrt{\frac{j\omega\mu_0}{\sigma}}, \tag{13}$$

on the target boundary. $J_S(\cdot)$ in equation (13) can be solved by the moment method [20]. After $J_S(\cdot)$ is solved, the scattered electric field of equation (10) will be obtained accordingly.

The goal of inverse scattering is to obtain the target shape function $f(\phi)$, which is unknown in practical applications. To help reconstruction, the target shape function $f(\phi)$ should be approximated and controlled by some variables. As the target shape is smooth, it can be well approximated by a Fourier series and controlled by Fourier coefficients, as given in [15, 16, 18]. This study considers the target with a complex shape, e.g., containing corners. In such a situation, the Fourier bases are too smooth and are then inadequate to model the target shape. Instead, this study utilizes the cubic spline interpolation [21, 22] to model the target with a complex shape. Initially, we expand the polar coordinate angle (ϕ) into a horizontal axis with the range $[0, 2\pi]$. Next, the horizontal range $[0, 2\pi]$ is equally divided into M

segments with division points at $\phi_i = i \cdot 2\pi/M$, $i = 0, 1, 2, \ldots, M$. The target shape function is then sampled at these division points and the results are $f(\phi_i)$, $i = 1, 2, \ldots, M$. Note that $f(\phi_0)$ is unnecessary due to $f(\phi_0) = f(\phi_M)$. Figure 4 illustrates four of the whole sampling points in the cubic spline interpolation. As shown in Figure 4, $f(\phi)$ in $\phi_{i-2} < \phi < \phi_{i-1}$, $\phi_{i-1} < \phi < \phi_i$ and $\phi_i < \phi < \phi_{i+1}$ are approximated by cubic polynomials $S_{i-1}(\phi)$, $S_i(\phi)$, and $S_{i+1}(\phi)$, respectively. According to the cubic spline interpolation [21, 22], the cubic polynomial functions $S_1(\phi)$, $S_2(\phi)$, ..., and $S_M(\phi)$ within adjacent points can be determined from the $(M+1)$ sampling points $(\phi_0, f(\phi_0))$, $(\phi_1, f(\phi_1))$, $(\phi_2, f(\phi_2))$, ..., and $(\phi_M, f(\phi_M))$. The details are given in [21, 22]. Note that $f(\phi_0)$, $f(\phi_1)$, $f(\phi_2)$,..., and $f(\phi_M)$ are known because one should guess their values consecutively in the WOA iteration of Section 2. As all cubic polynomial functions are determined, the target shape function $f(\phi)$ is then approximated as

$$f(\phi) \cong \begin{cases} S_1(\phi), & 0 \le \phi \le \phi_1, \\ S_2(\phi), & \phi_1 \le \phi \le \phi_2, \\ \vdots & \vdots \\ S_M(\phi), & \phi_{M-1} \le \phi \le \phi_M = 2\pi. \end{cases} \tag{14}$$

As mentioned above, the inverse scattering should be first transformed into a minimization problem. The fitness (objective) function is based on the difference of scattered electric fields between the guessed and true targets. To make the inversion reliable, we illuminate the target from different directions including $\alpha = 0^\circ$, 90°, 180°, and 270°, respectively. For each incidence, the scattered electric fields are collected in eight directions, which are $\phi = 0^\circ$, 45°, 90°, ..., and 315°, respectively. Thus we totally collect 32 $(=4 \times 8)$ data sets of scattered electric fields. As these scattered electric fields are collected from the true target, they are recorded as Ans(1), Ans(2), ..., and Ans(32). The goal is to obtain $f(\phi_i)$, $i = 1, 2, \ldots, M$, and conductivity σ by comparing the 32 collected data sets of scattered electric fields. Thus the total number of controlled variables in the minimization problem is $(M+1)$. During the WOA iteration in Section 2, one should guess values for these $(M+1)$ variables and approximate the shape function from the cubic spline interpolation as equation (14). Thus one can solve $J_S(\cdot)$ in equation (13) by the moment method and then calculate the corresponding scattered electric field from equation (10). The scattered electric fields from the guessed target are calculated under the same situations of incidence and collection as mentioned above. The results are recorded as Guess(1), Guess(2), ..., and Guess(32). The fitness (objective) function is defined as

$$\text{fitness} = \left\{ \frac{1}{32} \sum_{i=1}^{32} \left| \frac{\text{Guess}(i) - \text{Ans}(i)}{\text{Ans}(i)} \right|^2 \right\}^{1/2}. \tag{15}$$

The inverse scattering becomes to find optimum values of $f(\phi_i)$, $\phi_i = i \cdot 2\pi/M$ $(i = 1, 2, \ldots, M)$ and conductivity σ that minimizes equation (15). In this study, the above minimization procedures are implemented by the whale optimization algorithm in Section 2. As the optimum values of the $(M+1)$ controlled variables are obtained, the true target shape can be reconstructed from equation (14) and its conductivity is also known simultaneously. Therefore, the inverse scattering is achieved.

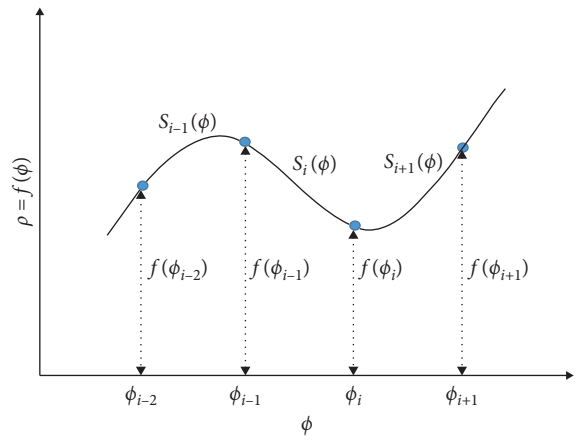

Figure 4: Illustration of the cubic spline interpolation.

4. Numerical Results

In this section, numerical examples are given to illustrate the application of whale optimization algorithm in inverse scattering. Consider an imperfectly conducting cylinder in free space illuminated by a plane wave of equation (9), as shown in Figure 3. The frequency of the incident wave is 300 MHz. The transmitting and receiving details have been mentioned in Section 3. The distance between each receiver and the coordinate origin is chosen as 12 m. Note that the scattered electric field is calculated by equation (10), which is suitable for both near and far fields. Therefore, the choice of distance between a receiver and the coordinate origin is not important. The conductivity of the target is $\sigma = 5.8 \times 10^7$ S/m, which implies that the target is made of copper. In the cubic spline interpolation of Section 3, the angle range $[0, 2\pi]$ is equally divide into 16 segments, i.e., $M = 16$. In the whale optimization algorithm, the dimension of each location vector is 17. The 17 components of a location vector represent 16 sampling values of the target shape function and one value for conductivity. The population size is chosen as $N_W = 15$. The b value for defining the shape of the logarithmic spiral in equation (5) is chosen as $b = 1$. All length units are meters. In the following, there are two examples to illustrate the above inverse scattering scheme. The whale optimization algorithm is inherently a randomness iteration algorithm so that the simulation should be done many times. In the following, each example is simulated 30 times and all illustrated figures are the average results.

In the first example, the shape of the target is similar to a star, as the black line marked "True shape" in Figure 5. The values of sampling points for the true target shape function, i.e., $(\phi_i, f(\phi_i))$ for $\phi_i = i \cdot 2\pi/16$, $i = 1, 2, \ldots, 16$, are listed in the first and second columns of Table 2. Following the WOA and inverse scattering procedures in Section 2 and Section 3, the reconstructed target shape for different iteration loops of

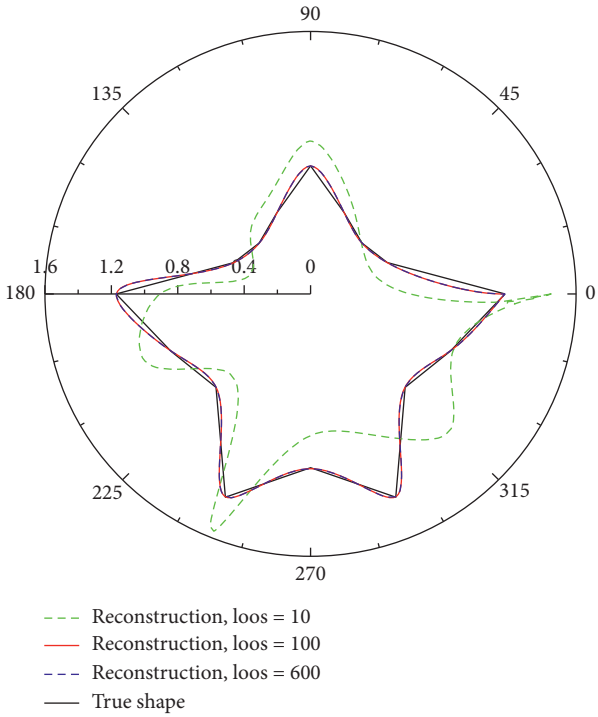

Figure 5: Reconstructed target shape for different iteration loops of the whale optimization algorithm in the first example.

Table 2: Values of sampling points ($M = 16$) for the true target shape function in the first (Ex1) and second (Ex2) examples.

$\phi_i = i \cdot 2\pi/16$	$f(\phi_i)$ for Ex1	$f(\phi_i)$ for Ex2
$1 \cdot 2\pi/16$	0.4999	0.5673
$2 \cdot 2\pi/16$	0.4382	0.2362
$3 \cdot 2\pi/16$	0.5332	0.8326
$4 \cdot 2\pi/16$	0.7808	0.6749
$5 \cdot 2\pi/16$	0.5332	0.2361
$6 \cdot 2\pi/16$	0.4382	0.1422
$7 \cdot 2\pi/16$	0.4999	0.1212
$8 \cdot 2\pi/16$	1.1712	0.5431
$9 \cdot 2\pi/16$	0.9111	0.4615
$10 \cdot 2\pi/16$	0.8055	0.8801
$11 \cdot 2\pi/16$	1.3408	0.3692
$12 \cdot 2\pi/16$	1.0591	0.9388
$13 \cdot 2\pi/16$	1.3408	0.4878
$14 \cdot 2\pi/16$	0.8055	0.4285
$15 \cdot 2\pi/16$	0.9110	0.8993
$16 \cdot 2\pi/16$	1.1712	0.4351

the whale optimization algorithm is shown in Figure 5. It reports that the target shape is well reconstructed as the number of iteration loops is larger than 100. The fitness value with respect to iteration loops of the whale optimization algorithm is shown in Figure 6. As defined in (15), the fitness value is always positive and the goal is to reach 0. Figure 6 shows that the fitness becomes very small after only dozens of iteration loops. This means that our inverse scattering based on the whale optimization algorithm converges very fast. To investigate the reconstruction accuracy, we define the relative shape error as

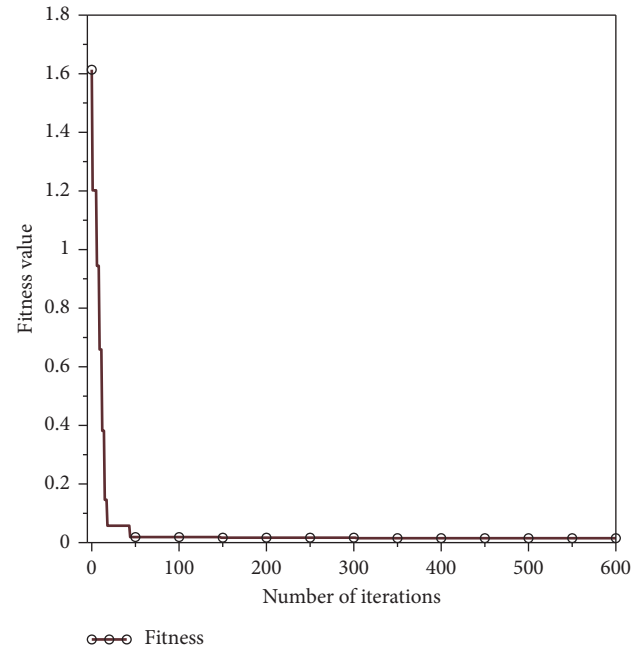

Figure 6: The fitness value with respect to iteration loops of the whale optimization algorithm for the first example.

$$\mathrm{SE} = \left\{ \frac{1}{360} \sum_{i=1}^{360} \left| \frac{f_R(i \cdot 2\pi/360) - f_T(i \cdot 2\pi/360)}{f_T(i \cdot 2\pi/360)} \right|^2 \right\}^{1/2}, \tag{16}$$

where $f_R(\cdot)$ and $f_T(\cdot)$ denote the shape function values for the reconstructed and true targets, respectively. In addition, we define the relative conductivity error as

$$\mathrm{CE} = \left| \frac{\sigma_R - \sigma_T}{\sigma_T} \right|, \tag{17}$$

where σ_R and σ_T denote values of the reconstructed and true conductivity, respectively. Obviously, the values for both equations (16) and (17) are always positive and the goal is to reach 0. Figure 7 shows the relative shape and conductivity errors with respect to iteration loops of the whale optimization algorithm. It shows that the reconstruction is very consistent, i.e., the relative error approaches 0, after only dozens of iteration loops.

In the second example, the shape of the target is similar to a maple leaf, as the black line marked "True shape" in Figure 8. The values of sampling points for the true target shape function, i.e., $(\phi_i, f(\phi_i))$ for $\phi_i = i \cdot 2\pi/16$, $i = 1, 2, \ldots, 16$, are listed in the first and third columns of Table 2. The other conditions are the same as those of the first examples. Figure 8 reports the reconstructed target shape for different iteration loops of the whale optimization algorithm. Like the first example, the target shape is well reconstructed as the number of iteration loops is larger than 100. Figure 9 reports the fitness value with respect to iteration loops of the whale optimization algorithm. It shows that the fitness becomes very small as the number of iteration loops is greater than 100. Like the first example, the convergence is also very fast

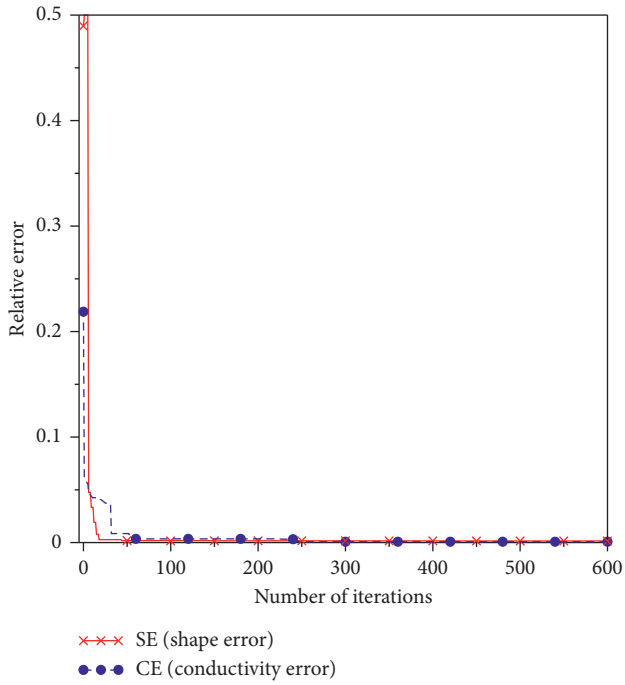

Figure 7: The relative shape and conductivity errors with respect to iteration loops of the whale optimization algorithm for the first example.

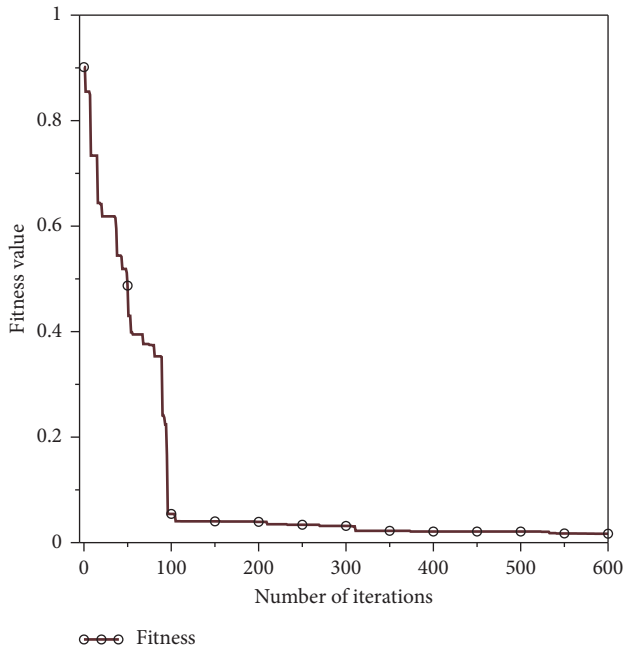

Figure 9: The fitness value with respect to iteration loops of the whale optimization algorithm for the second example.

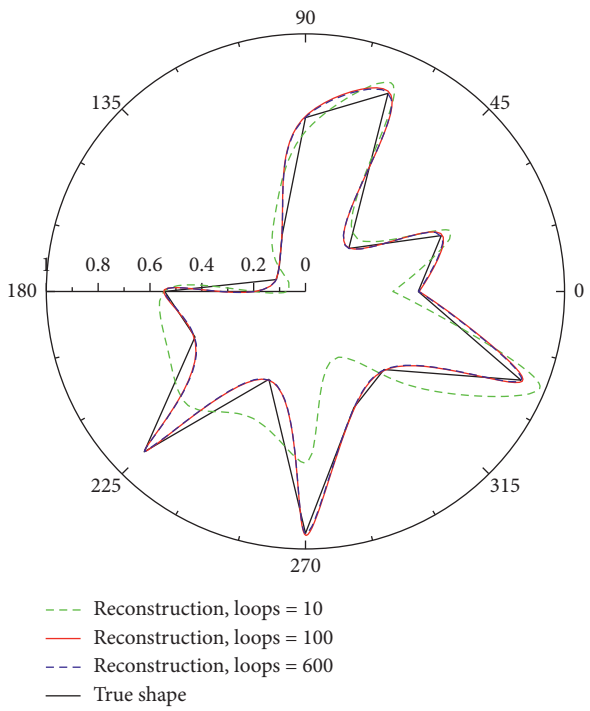

Figure 8: Reconstructed target shape for different iteration loops of the whale optimization algorithm in the second example.

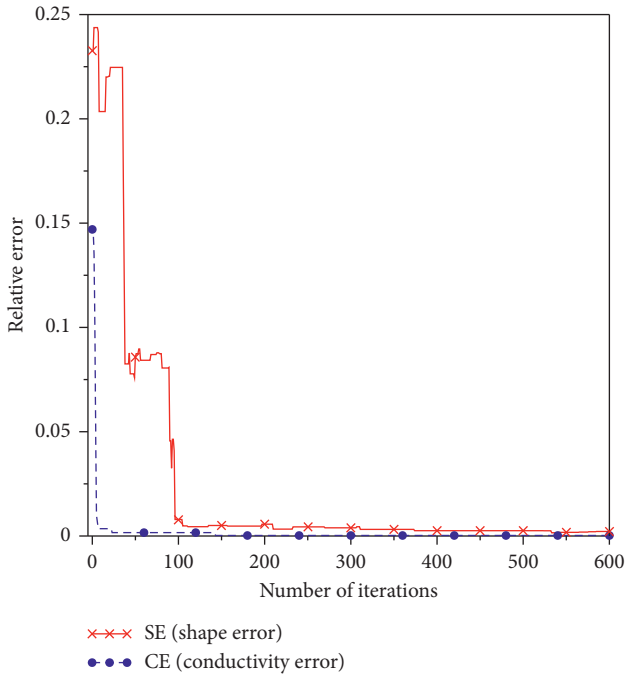

Figure 10: The relative shape and conductivity errors with respect to iteration loops of the whale optimization algorithm for the second example.

in this example. Figure 10 reports the relative shape and conductivity errors with respect to iteration loops of the whale optimization algorithm. It shows that the reconstruction is very consistent, i.e., the relative error approaches 0, as the number of iterations is greater than 100. Note that the WOA iteration is to minimize the fitness in equation (15), but not the relative reconstruction error in equations (16) and (17). Therefore, the curves in Figure 10 may have some ripples although the overall trend is decreasing.

The above results show that the overall convergence of the second example is a little slower than that of the first example. This may be because the target shape and then scattering mechanisms of the second example (a maple leaf) are more complex than those of the first example (a star). Although the scale for each target of the above simulation is small, our research flowchart has no limitation on the target scale. As the target become larger, one only needs to increase the number of segments in moment method solution for equation (13) and the number of segments in shape function division (i.e., M in cubic spline interpolation or Table 2). The above inverse scattering is limited to homogeneous scatterers. As the target is inhomogeneous, the above homogeneous scattering formulas in equations (10)–(13) should be replaced by inhomogeneous scattering theories [25]. Under such a situation, the induced surface current density $J_S(\cdot)$ in equations (10)–(13) will be extended to the whole target volume so that the number of variables in moment method analysis is greatly increased. The other reconstruction procedures of the target are almost the same except that the computation is more time-consuming. The above simulation is implemented on a personal computer with Intel Core i7-4720HQ CPU and 16 GB RAM. The software includes Windows 10 operation systems, Microsoft Visual C++ 2010 programming language and IMSL Math Library.

5. Conclusion

In [19], the WOA was conducted on 29 mathematical benchmark functions. It has been found to be enough competitive with other state-of-the-art metaheuristic methods and superior over many conventional techniques [19]. This study further applies the WOA to the inverse scattering of an imperfectly conducting target with corners. The results are successful and satisfactory. The forward problem of this study involves scattering integral equations with Green's functions, which are complicated and difficult. To obtain the target information, i.e., inverse scattering, the problem is successfully transformed into a nonlinear optimization problem, which can be well treated by the WOA. The WOA iteration guesses the target's shape and conductivity until the scattered electric fields of the guessed target are consistent with (or at least close to) those of the true target. Numerical results show that our WOA based inverse scattering is not only accurate but also converges fast. The WOA can also be extended to solve many other nonlinear and complicated problems in electromagnetic waves.

Data Availability

The important and key computer programs of this study are available online, http://myweb.ncku.edu.tw/~kclee/program-InvSca_20191003.zip.

Conflicts of Interest

The authors declare that they have no conflicts of interest.

Acknowledgments

The authors would like to thank the financial support from the Ministry of Science and Technology, Taiwan, under Grant MOST 108-2221-E-006-091 and the National Center for High Performance Computing, Taiwan, for computer time and facilities.

References

[1] H. L. Zhou, Y. W. Liu, Y. H. Wang, L. B. Chen, and R. X. Duan, "Nonlinear electromagnetic inverse scattering imaging based on IN-LSQR," *International Journal of Antennas and Propagation*, vol. 2018, Article ID 2794646, 9 pages, 2018.

[2] C. Estatico, A. Fedeli, M. Pastorino, A. Randazzo, and E. Tavanti, "Microwave imaging of 3D dielectric structures by means of a Newton-CG method in spaces," *International Journal of Antennas and Propagation*, vol. 2019, Article ID 2841937, 14 pages, 2019.

[3] C. A. Balanis, *Advanced Engineering Electromagnetics*, Wiley, New York, NY, USA, 1989.

[4] R. Lewis, "Physical optics inverse diffraction," *IEEE Transactions on Antennas and Propagation*, vol. 17, no. 3, pp. 308–314, 1969.

[5] N. H. Farhat, T. Dzekov, and E. Ledet, "Computer simulation of frequency swept imaging," *Proceedings of the IEEE*, vol. 64, no. 9, pp. 1453-1454, 1976.

[6] C. Chi and N. H. Farhat, "Frequency swept tomographic imaging of three-dimensional perfectly conducting objects," *IEEE Transactions on Antennas and Propagation*, vol. 29, no. 5, pp. 312–319, 1981.

[7] N. Bojarski, "A survey of the physical optics inverse scattering identity," *IEEE Transactions on Antennas and Propagation*, vol. 30, no. 5, pp. 980–989, 1982.

[8] D. B. Ge, "A study of the Lewis method for target-shape reconstruction," *Inverse Problems*, vol. 6, no. 3, pp. 363–370, 1990.

[9] A. Roger, "Newton-Kantorovitch algorithm applied to an electromagnetic inverse problem," *IEEE Transactions on Antennas and Propagation*, vol. 29, no. 2, pp. 980–989, 1981.

[10] A. Kirsch, R. Kress, P. Monk, and A. Zinn, "Two methods for solving the inverse acoustic scattering problem," *Inverse Problems*, vol. 4, no. 3, pp. 749–770, 1988.

[11] D. Colton and P. Monk, "A new method for solving the inverse scattering problem for acoustic waves in an inhomogeneous medium," *Inverse Problems*, vol. 5, no. 6, pp. 1013–1026, 1989.

[12] G. P. Otto and W. C. Chew, "Microwave inverse scattering—local shape function imaging for improved resolution of strong scatterers," *IEEE Transactions on Microwave Theory and Techniques*, vol. 42, no. 1, pp. 137–141, 1994.

[13] F. Hettlich, "Two methods for solving an inverse conductive scattering problem," *Inverse Problems*, vol. 10, no. 2, pp. 375–385, 1994.

[14] K.-C. Lee, "A neural-network-based model for 2D microwave imaging of cylinders," *International Journal of RF and Microwave Computer-Aided Engineering*, vol. 14, no. 5, pp. 398–403, 2004.

[15] K.-C. Lee, "Inverse scattering of a conducting cylinder in free space by modified fireworks algorithm," *Progress In Electromagnetics Research M*, vol. 59, pp. 135–146, 2017.

[16] K.-C. Lee, "Microwave imaging of a conducting cylinder buried in a lossless half space by modified fireworks

algorithm," *Microwave and Optical Technology Letters*, vol. 60, no. 6, pp. 1374–1381, 2018.

[17] K.-C. Lee and P.-T. Lu, "Inverse scattering of an imperfectly conducting cylinder with corners by firefly algorithms," *Electromagnetics*, vol. 38, no. 8, pp. 517–530, 2018.

[18] C. C. Chiu and P. T. Liu, "Image reconstruction of a perfectly conducting cylinder by the genetic algorithm," *IEE Proceedings—Microwaves, Antennas and Propagation*, vol. 143, no. 3, pp. 259–253, 1996.

[19] S. Mirjalili and A. Lewis, "The whale optimization algorithm," *Advances in Engineering Software*, vol. 95, pp. 51–67, 2016.

[20] R. F. Harrington, *Field Computation by Moment Methods*, Macmillan, New York, NY, USA, 1968.

[21] S. A. Dyer and J. S. Dyer, "Cubic-spline interpolation. 1," *IEEE Instrumentation & Measurement Magazine*, vol. 4, no. 1, pp. 44–46, 2001.

[22] S. A. Dyer and X. He, "Cubic-spline interpolation: part 2," *IEEE Instrumentation & Measurement Magazine*, vol. 4, no. 2, pp. 34–36, 2001.

[23] C. C. Chiu and Y. W. Kiang, "Electromagnetic imaging for an imperfectly conducting cylinders," *IEEE Transactions on Microwave Theory and Techniques*, vol. 39, no. 9, pp. 1632–1639, 1991.

[24] E. C. Jordan and K. G. Balmain, *Electromagnetic Waves and Radiating Systems*, Prentice-Hall, Upper Saddle River, NJ, USA, 1968.

[25] W. C. Chew, *Waves and Fields in Inhomogeneous Media*, IEEE press, Piscataway, NJ, USA, 1995.